An update to this article is included at the end

International Journal of Biological Macromolecules 316 (2025) 144436

Contents lists available at ScienceDirect

International Journal of Biological Macromolecules

journal homepage: www.elsevier.com/locate/ijbiomac

Transformative lactera-polypyrrole@carrageenan microparticles leveraging NIR for skin regeneration and stress relief

Sih-Chi Chuang [a,b,1], Shih-An Yu [c,1], Pei-Chia Hung [c,1], Andrew E.-Y. Chuang [d,e,f,1], Jia-Wei Liang [c,d,1], Lekshmi Rethi [d,e,1], Chih-Kuang Chen [g,h,i], Hsu-Wei Fang [a], Hieu Trung Nguyen [j], Hsien-Tsung Lu [k,l,m,*]

[a] Department of Chemical Engineering and Biotechnology, National Taipei University of Technology, Taipei 10608, Taiwan
[b] Doctoral Program of Biochemical and Biomedical Engineering, National Taipei University of Technology, Taipei 10608, Taiwan
[c] Hsuan Chen Technology CO., LTD., New Taipei City 22055, Taiwan
[d] Graduate Institute of Biomedical Materials and Tissue Engineering, College of Biomedical Engineering, Taipei Medical University, New Taipei City, Taiwan
[e] International Ph.D. Program in Biomedical Engineering, College of Biomedical Engineering, Taipei Medical University, New Taipei City, Taiwan
[f] Cell Physiology and Molecular Image Research Center, Taipei Medical University-Wan Fang Hospital, Taipei 11696, Taiwan
[g] Department of Physical Medicine and Rehabilitation, Chang Gung Memorial Hospital, Taoyuan, Taiwan.
[h] School of Medicine, Chang Gung University, Taoyuan, Taiwan.
[i] Graduate Institute of Clinical Medicine, College of Medicine, Taipei Medical University, Taipei, Taiwan.
[j] Department of Orthopedics and Trauma, Faculty of Medicine, University of Medicine and Pharmacy at Ho Chi Minh City, Ho Chi Minh City 700000, Viet Nam
[k] Department of Orthopedics, Taipei Medical University Hospital, Taipei City 11031, Taiwan
[l] Department of Orthopedics, School of Medicine, College of Medicine, Taipei Medical University, Taipei 11031, Taiwan
[m] International Ph.D. Program in Cell Therapy and Regenerative Medicine, College of Medicine, Taipei Medical University, Taipei 11031, Taiwan

A B S T R A C T

Effective wound healing remains a significant challenge in regenerative medicine, particularly in minimizing inflammation and promoting scarless recovery. This study introduces a bioengineered LAC-PPy@Car MF composite, designed to leverage near-infrared (NIR)-induced photothermal therapy alongside biotherapeutics to facilitate tissue regeneration. The composite integrates the photothermal properties of polypyrrole (PPy) with the anti-inflammatory and regenerative potential of Lactera (LAC) and Carrageenan (Car). Upon NIR activation, the composite generates localized mild-hyperthermia, reducing oxidative stress, enhancing Aryl Hydrocarbon Receptor (AhR) activity, and upregulating heat shock proteins (HSP). These effects synergistically create a bioactive environment conducive to cellular proliferation and tissue repair. Biochemical evaluations demonstrate that LAC-PPy@Car MF effectively reduces oxidative stress, stimulates fibroblast migration, and promotes the proliferation of skin cells. Immunofluorescence staining reveals significant activation of AhR and HSP in treated tissues, correlating with cellular proliferation and improved skin architecture. The NIR-triggered photothermal effect contributes to the therapeutic potential of the composite, ensuring precise and minimally invasive treatment for burn injuries. These findings position phototherapeutic LAC-PPy@Car MF as a promising candidate for advanced wound healing applications. Its dual functionality, combining photothermal therapy with bioactive healing properties, offers a transformative approach to regenerative medicine, paving the way for improved clinical outcomes in wound care.

1. Introduction

Wound healing is a complex biological process influenced by inflammation, tissue remodeling, and cellular regeneration. As the body's largest organ, the skin and its appendages serve as critical barriers against physical injury, which poses significant public health risks [1,2]. When skin integrity is compromised, additional protective measures are essential to shield the wound [3]. Clinically, strategies such as debridement and the application of specialized wound dressings are employed to promote healing. The ideal dressings not only prevent secondary infections but also accelerate skin barrier restoration [4,5]. However, a major challenge in skin repair is the formation of fibrotic scar tissue, which lacks the functionality of normal skin and reduces both strength and flexibility [6–8]. Achieving scarless wound healing remains a critical clinical objective.

Inflammation plays a key role in wound healing [9]. While fibroblasts and keratinocytes produce cytokines to regulate immune responses, excessive inflammation can lead to further tissue damage

* Corresponding author at: Department of Orthopedic, Taipei Medical University Hospital, Taipei City 11031, Taiwan.
E-mail address: lu7788@tmu.edu.tw (H.-T. Lu).
[1] These authors contributed equally.

https://doi.org/10.1016/j.ijbiomac.2025.144436
Received 12 December 2024; Received in revised form 16 April 2025; Accepted 19 May 2025
Available online 20 May 2025
0141-8130/© 2025 Elsevier B.V. All rights are reserved, including those for text and data mining, AI training, and similar technologies.

[10,11]. Rapid anti-inflammatory intervention in the early stages of skin restoration is crucial it can prevent the excessive accumulation of inflammatory cells, suppress cytokine storms, and mitigate additional wound injury [12]. In response, innovative functional wound dressings have been developed, including porous foams [13], hydrogels [14–16], and micro-sized matrices [17,18]. These solutions feature biomimetic extracellular matrix-like structures [19–22] that support cellular functions essential for effective healing [23–25].

Recent studies have demonstrated that heat shock proteins (HSPs) offer protection against mitochondrial damage, apoptosis, oxidative stress, and inflammation. Overexpression of HSPs can reduce oxidative stress–induced cell death and modulate key processes such as inflammation, cell proliferation, migration, and collagen synthesis making them indispensable for wound healing [26]. Additionally, the Aryl Hydrocarbon Receptor (AhR), a ligand-dependent transcription factor, has been implicated in wound healing by mediating the biological effects of both natural and synthetic compounds [27,28].

Combining photothermal therapy (PTT) with chemotherapy has shown promising results in the treatment of skin diseases, delivering effective therapy with minimal systemic toxicity [29–31]. Porous carbon-based agents have garnered attention for their biocompatibility and efficiency as near-infrared (NIR) laser absorbers, facilitating photothermal conversion and targeted drug delivery [32,33]. Conductive polymers, such as polypyrrole (PPy), are increasingly used as multifunctional materials; however, conventional polymerization methods may raise biotoxicity concerns, highlighting the need for safer formulations [34–37]. Moreover, electroactive hydrogels can rapidly restore electrical signal transmission, which is critical for cell recruitment, migration, and proliferation during wound healing [38,39]. Advanced dressings with engineered topographies further enhance cellular responses: anisotropic structures guide cell orientation and migration [40], while random topographies influence various cellular behaviors [41]. Additionally, temperature-responsive polymeric materials offer the potential for programmable reconfigurations during PTT, enabling precise cell manipulation [42,43].

Recent advances in biomaterial science have paved the way for the development of innovative wound dressings tailored for diverse wound types. In particular, carrageenan-based dressings have garnered considerable attention due to their biodegradability, biocompatibility, and minimal cytotoxicity. Their superior physico-mechanical properties make them especially effective for wounds with high levels of exudate, with bioprocessing techniques emerging as a promising method to enhance their performance [44]. Further research has revealed that soy active substances can significantly accelerate wound healing by boosting dermal extracellular matrix synthesis and promoting re-epithelialization. The critical contributions and potential of soy-based materials for wound repair have been thoroughly examined in the literature [45]. Moreover, recent studies have demonstrated the efficacy of utilizing topical probiotics in a soybean-based concentrate (Lactera, LAC) to manage diabetic foot ulcers [46].

Dynamic changes in biomarkers—such as HSP, AhR, inflammatory oxidative stress, and proliferative activation—in biomaterial-treated wounds are critical yet underexplored. Therefore, it is essential to perform an in-depth study to fully understand these alterations and their implications for wound healing. In this context, our study introduces a novel, temporally tunable oxygen-crosslinked microparticle system (LAC-PPy@Car MF) designed for enhanced tissue repair (**Scheme 1**.). Unlike conventional biomaterials that lack spatial and temporal responsiveness, our system leverages the controlled oxidative polymerization of pyrrole using CaO_2 and LAC to form a stable polypyrrole-based composite with sustained photothermal and biological activity. Time-dependent analyses reveal that this formulation not only maintains colloidal stability and oxidative potential over several days but also supports progressive cellular proliferation, AhR activation, and HSP expression—each peaking at defined intervals. Furthermore, in vivo wound healing assessments confirm that the NIR-activated LAC-PPy@Car MF composite promotes early epidermal regeneration and accelerates the resolution of inflammation, with marked temperature elevation and histological improvements observed within the first two weeks.

Driven by a hypothesis that synchronizing the physicochemical and biological effects of wound dressings with the dynamic phases of wound healing can significantly enhance tissue repair, our study presents an innovative, multifunctional composite. This time-resolved system establishes a robust platform for next-generation regenerative therapies, inspiring new directions in both fundamental research and clinical application.

2. Experimental section

2.1. Materials

In the studies, we utilized several reagents: Pyrrole (Py), 4′,6-diamidino-2-phenylindole (DAPI), Car, Fluorescein Isothiocyanate (FITC), Calcium Peroxide (CaO_2), and Propidium iodide (PI), all sourced from sigma-Aldrich, St. Louis, MO, USA. The L929 fibroblast cell line was obtained from the American Type Culture Collection (ATCC), which is a standard choice for biomedical research due to its robust growth characteristics and well-documented genomic profile.

We employed the Live/Dead assay for cell viability, acquiring this kit from Thermo Fisher Scientific, USA. Fluorescently labeled antibodies

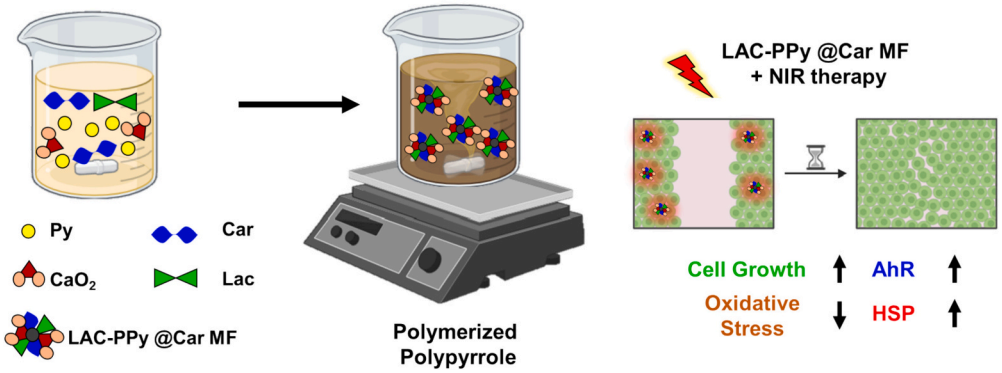

Scheme 1. Schematic representation of the formulation and function of the LAC-PPy@Car MF composite. *(Left)* The synthesis process involves combining calcium peroxide (CaO_2), Lactera (LAC), pyrrole (Py), and carrageenan (Car) under magnetic stirring to produce uniform, water-soluble, near-infrared (NIR)-responsive microparticles. *(Right)* The composite's functional effects are illustrated by comparing untreated and treated conditions. Upon NIR activation, LAC-PPy@Car MF generates localized heat, which enhances cell proliferation (green), reduces oxidative stress (orange), activates AhR (blue), and increases HSP expression (red), thereby promoting skin regeneration and mitigating inflammation. The illustration was made using BioRender.

specifically targeting the aryl hydrocarbon receptor (AhR) and RH123 were provided by Ab-science Co., Ltd. in Taipei, Taiwan. Additionally, Lactera (LAC), a soybean concentrate, was supplied by Bao Geng Biotechnology Co., Taiwan. These materials are critical for executing a diverse array of biochemical and cellular studies, particularly in cellular imaging and viability assessments.

The experimental setups included fetal bovine serum from Bioidea, 1 % streptomycin/penicillin from Gibco (Thermo Fisher Scientific, USA), DMEM (Dulbecco's Modified Eagle Medium) from Gibco (Thermo Fisher Scientific, USA), dimethyl sulfoxide (DMSO) from Merck, and the Calcein AM/ethidium homodimer-1 (EthD-1) kit from Biotium, UK.

2.2. Formulation as well as characterization

To optimize the formulation, a series of experiments examining various mass ratios of LAC, Car, CaO_2, and Py was performed. The specific ratios investigated included 10/5/3/30, 10/5/6/30, 10/5/9/30, 10/5/12/30, and 10/5/15/30 (LAC/Car/Py/CaO_2). The aqueous components were mixed thoroughly with a magnetic stirrer at 100 RPM under ambient conditions. Post-mixing, Dynamic Light Scattering (DLS) was exploited to evaluate the particle size distribution, Polydispersity Index (PDI), and zeta potential.

To investigate structural modifications within the formulations, we introduced FITC fluorescent dye at a concentration of 1 mg/mL during preparation. Morphological changes were determined using fluorescence microscopy. Additionally, the Oxidation-Reduction Potential (ORP) was applied to determine the oxidation-reduction states of the samples. Spectrometric techniques were utilized to evaluate the degree of polymerization, while Fourier Transform Infrared Spectroscopy (FTIR) was used to provide insights into chemical characteristics. X-ray diffraction (XRD) was utilized to evaluate the crystallite characteristics. Temperature measurements were carried out to assess photothermal effects under NIR irradiation.

Temperature assessments under NIR exposure further enhance our understanding of the thermal characteristics of the formulations. A thermal cycling experiment was performed to evaluate the stability and reusability of the Lac-PPy@Car MF composite under NIR light exposure. The NIR light was turned on and off at 3-minute intervals over a total duration of 9 min, and the temperature changes were recorded to assess the material's photothermal performance and reproducibility.

2.3. In vitro appraisals

The cytotoxicity of the formulations was evaluated using L929 fibroblast cells at passage 17. Sterilized underwent a 20-minute UV radiation exposure within a clean bench environment. Approximately 10^4 cells were seeded per well. The cultures were incubated at 37 °C in 5 % CO_2 with Dulbecco's Modified Eagle Medium supplemented with 10 % fetal bovine serum and 1 % streptomycin/penicillin.

Cell proliferation assessment was conducted using the MTT assay. After a 24-hour incubation period, MTT solution (0.5 mg/mL in PBS) was added, and the resultant formazan crystals were solubilized in dimethyl sulfoxide before measuring absorbance at 490 nm with a Bio-Rad microplate reader. Additionally, cell viability was determined through a Live/Dead assay utilizing the Calcein AM/ethidium homodimer-1 (EthD-1) kit, adhering to the manufacturer's protocol. Furthermore, the cellular expression of aryl hydrocarbon receptors (AhRs) was analyzed via antibody detection during microscopic assessment.

In the cell migration assay, fibroblasts were exposed to the LAC-PPy@Car MF solution. Concurrently, the cells were subjected to NIR light. Time-lapse imaging was performed at regular intervals, typically every 2 h, using a live cell imaging system

2.4. In vivo appraisals

For appraising the wound healing and scar-reducing effects of the LAC-PPy@Car MF combined with NIR-PTT, a in vivo burn wound model was created. ICR mice (ca. 20 g) were obtained from BioLASCO (Taipei, Taiwan). All experimental procedures were approved by the Institutional Animal Care and Use Committee of Taipei Medical University. Once inducing anesthesia by 1–4 % of inhalation of isoflurane, the dorsal hair of the mice was shaved carefully. A deep second-degree burn wound (about 1 cm in diameter) was made onto the dorsal skin of animals.

For comparing the effects of the LAC-PPy@Car MF combined with NIR irradiation (LAC-PPy@Car MF + NIR) on wound healing, control groups were included: the normal group, burn wound + NIR, burn wound + LAC-PPy@Car MF (topical injection), and burn wound + LAC-PPy@Car MF (topical injection) + NIR.

Wounds underwent disinfection, photography, and re-bandaging until complete healing was confirmed. In the LAC-PPy@Car MF + NIR cohort, NIR irradiation at a dose of 1.0 W/cm^2 and a wavelength of 600-900 nm was applied daily for 5 min. In a 14-day post-treatment period, various tissues, including skin, heart, liver, spleen, lung, and kidney, were harvested for fixation, sectioning, and hematoxylin and eosin (HE) histological evaluation. The skin tissues subjected to treatment were further analyzed via immunofluorescence staining utilizing commercial antibodies for HSP and AhR, along with 5-Ethynyl-2′-deoxyuridine (EDU) and Tumor Necrosis factor-α assays. Cellular nuclei were counterstained with propidium iodide (PI) or 4′,6-diamidino-2-phenylindole (DAPI) for enhanced visualization.

2.5. Statistical analysis

Differences were assessed using the software of GraphPad Prism. Statistically significant differences were considered for $*p \leq 0.05$, $**p \leq 0.01$, $***p \leq 0.001$ and $****p \leq 0.0001$.

3. Results and discussion

Contemporary research is intensively examining the utility of oxygen-crosslinked materials within polymeric formulations aimed at enhancing tissue engineering scaffolds. These materials are distinguished by their customizable viscoelastic features, biocompatibility, and precisely controllable degradation rates. This investigation focused on the oxidative polymerization of Py, combined in formulations with CaO_2 and LAC. The resultant creation of ionomeric composites boasting varied chemical properties underlines the potential of these systems to engineer bioscaffolds that effectively replicate the mechanical and biological nuances of native tissue structures.

Utilizing oxygen biomaterial as a crosslinker enriches the polymers' biocompatibility and biological activity, fostering cell adhesion and growth, and offering controlled erosion rates that synchronize with natural tissue healing. The meticulous composition of Car, CaO_2, and LAC in the polymerization process permits fine-tuning of the composites' features, meeting the precise demands of sophisticated medical and biotech applications.

In Fig. 1**a**, we calculated the ratios of LAC, Car, Py, and CaO_2 to be 10/5/3/30, 10/5/6/30, 10/5/9/30, 10/5/12/30, and 10/5/15/30 in the formulation evaluations. An increase in CaO_2 level from 3 mg to 9 mg was shown to cause a considerable drop in particle size, reducing it from around 2400 nm to 1400 nm. The particle size of CaO_2 varies depending on its concentration, stabilization method, and grinding process. Higher concentrations and certain stabilizers, tend to produce larger particles approaching 2000 nm. CaO_2 concentrations also influence morphology, with particles exhibiting different shapes. Additionally, modified CaO_2 forms nanoscale particles but tends to aggregate quickly. These findings highlight that CaO_2 concentration and processing techniques play a crucial role in controlling particle size and stability

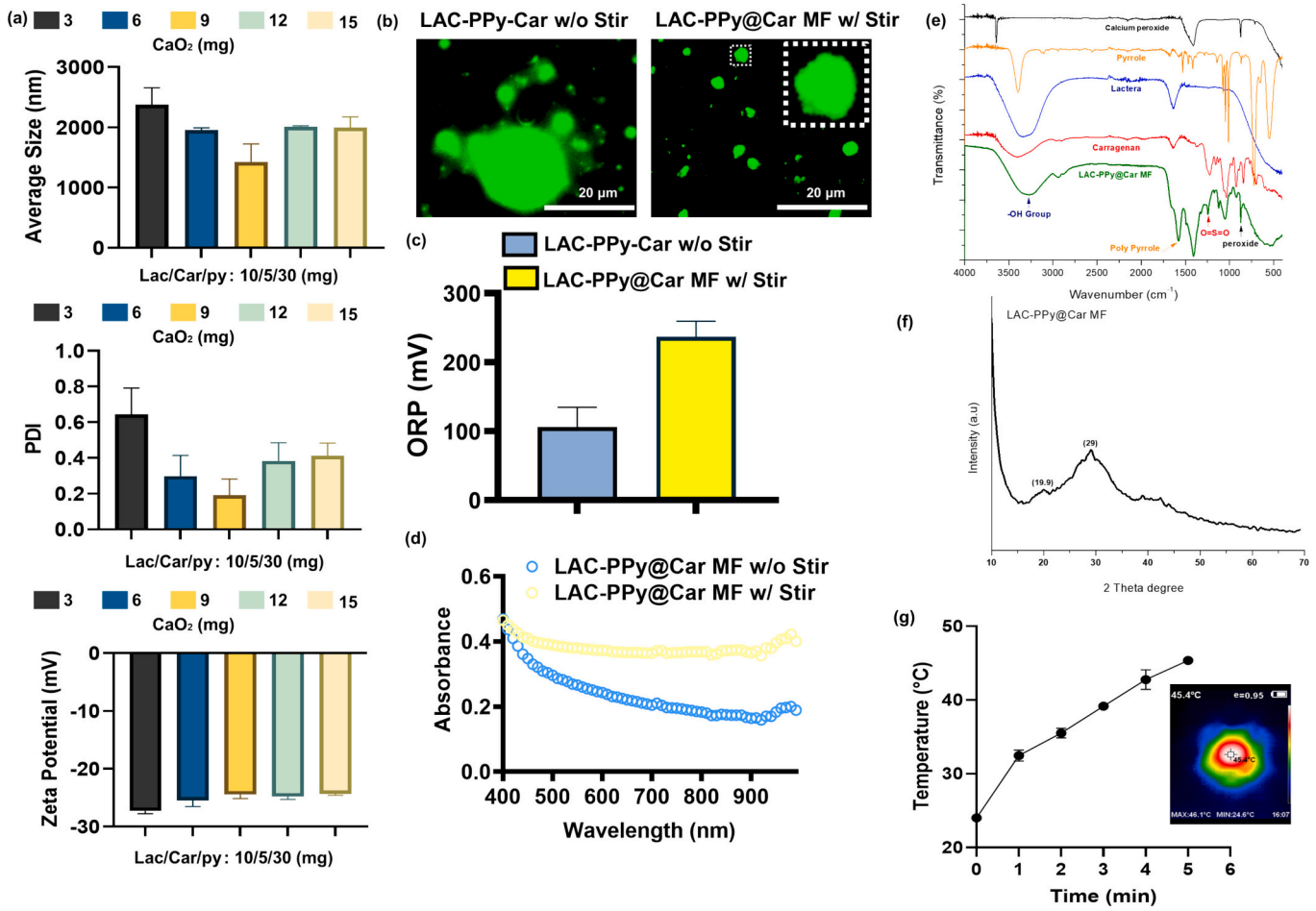

Fig. 1. (a) Dynamic light scattering (DLS) results showing the particle size, polydispersity index (PDI), and zeta potential of LAC-PPy@Car microparticles synthesized with various ratios of LAC/Car/CaO_2/Py (10/5/3/30, 10/5/6/30, 10/5/9/30, 10/5/12/30, and 10/5/15/30). (b) Fluorescence microscopy images comparing stirred and non-stirred formulations, highlighting the improved particle homogeneity and colloidal stability achieved with magnetic stirring. (c) Oxidation-reduction potential (ORP) measurements show higher oxidation levels in stirred formulations due to enhanced polymerization facilitated by CaO_2 and LAC. (d) UV–vis spectroscopy analysis of stirred and non-stirred formulations, demonstrating increased absorbance in the 400–900 nm range for stirred samples, confirming successful polypyrrole formation. (e) Fourier-transform infrared (FTIR) spectra of individual components and the final Lac-PPy@Car MF composite, revealing characteristic absorption bands indicative of successful chemical integration. (f) X-ray diffraction (XRD) patterns of the lac-PPy@Car MF composite, showing peaks corresponding to its structural characteristics. (g) Photothermal performance of the Lac-PPy@Car MF composite under NIR light, demonstrating temperature changes over 5 min, with a peak temperature of 45 °C, confirming its potential for photothermal therapy applications.

[47]. In the dispersion polymerization of particles, the particle size is primarily influenced by the solubility parameter of the reaction medium and the stabilizer concentration. Particle size tends to increase with the increasing polarity of the solvent mixture. A higher concentration of stabilizer leads to smaller particles and a greater total surface area, while an insufficient amount can result in particle aggregation. Increasing the initiator concentration generally produces slightly smaller and more numerous particles. The presence of oxygen before polymerization leads to a broad particle size distribution, whereas nitrogen-purged systems yield more uniform nanoparticles, particularly when the solubility parameter of the solvent mixture falls within an optimal range [48,49].

Dynamic Light Scattering (DLS) results (**Fig. 1a**) indicate the smallest particles were achieved at the mix ratio of LAC/Car/Py/CaO_2 of 10/5/9/30, selected for subsequent analyses. The polydispersity index (PDI) data (**Fig. 1a**) confirms the particles' uniformity below a PDI of ca. 0.2, and DLS zeta potential data (**Fig. 1a**) demonstrated a negative charge of approximately ranging from −20 to −30 mV, attributable to the anionic nature of the Car component.

The formulation and characterization of various ratios of the Car/Lac/Py/CaO_2 microparticles were systematically investigated to determine their physical properties, including particle size, polydispersity index (PDI), and zeta potential. For the ratio 10/5/30/3, the particle size was ca. 2400 nm, the PDI was ca. 0.65, and the zeta potential was ca. −27 mV. At the ratio 10/5/30/6, the particle size decreased to 1900 nm, with a PDI of ca. 0.30 and a zeta potential of ca. −25 mV. Further increasing the calcium peroxide to the ratio 10/5/30/9 resulted in a particle size of ca. 1400 nm, the lowest PDI of ca. 0.19, and a zeta potential of ca. −24 mV. For the ratio 10/5/30/12, the particle size was ca. 2000 nm, the PDI increased slightly to ca. 0.38, and the zeta potential remained at ca. −24 mV. At the highest tested ratio of 10/5/30/15, the particle size was ca. 2000 nm, with a PDI of ca. 0.41 and a zeta potential of ca. −24 mV. These results indicate that the particle size decreases with increasing calcium peroxide concentration up to 9, after which it stabilizes. The lowest PDI observed at the ratio 10/5/30/9 suggests a more uniform particle size distribution at this concentration and is picked for the following tests.

The literature mentioned that monomers such as thiophene, benzene, aniline, and pyrrole undergo chemical oxidative polymerization facilitated by oxidizing agents like CaO_2, noted for their role in hydrogen peroxide generation upon molecular interaction with water [50,51].

The anionic polymer known as Car is of great importance because of its unique structure, which consists of alternating units of hemisulfated

galactose and 3–6 anhydrogalactose. These units are connected by alpha 1➔3 and beta 1➔4 glycosidic linkages [52]. The sulfate ester groups of the polymer remain ionized even in normal physiological conditions, which guarantees its stability as an anionic polymer within the composite matrix. The car is offered in various variants, namely kappa, iota, and lambda, which are distinguished by their distinct patterns of sulfate esterification

Fluorescence microscopy data **(Fig. 1b)** displayed that the formulation composed of LAC/Car/CaO_2/Py at a ratio of 10/5/9/30 mg, when subjected to magnetic stirring, resulted in uniformly distributed microparticles demonstrating excellent colloidal stability. In contrast, the absence of magnetic stirring led to significant aggregation and precipitation of the particles, as evidenced by the microscopy data. This indicates that without stirring, the LAC-PPy@Car MF forms large particles, but with magnetic stirring, the particles become homogeneous and smaller in size. The application of magnetic stirring likely imparts essential shear forces that promote a microemulsion process, crucial for achieving the uniform dispersion and stability of the LAC-PPy@Car MF formulation. This uniform distribution of smaller particles is essential for the consistency and effectiveness of the formulation in potential applications.

The oxidation-reduction potential (ORP) data illustrated in **Fig. 1c** highlights that the formula exposed to magnetic stirring reached an ORP level above 200 mV, significantly higher than the non-stirred mixture which maintained an ORP around 100 mV. This disparity suggests that magnetic stirring enhances the interaction and surface contact among the formulation's components, facilitating a more thorough chemical reaction. Such reactions are likely fueled by the oxidative properties of CaO_2 and LAC, which contribute to the polymerization of Py, resulting in increased oxidation levels as supported by prior studies on chemical oxidative polymerization [53]. The ORP measurements exhibited a progressive increase over time, starting at 100 % on day 1, and further reaching 105 % on day 5, indicating a steady enhancement in the oxidative state of the system **(Fig. S1a)**.

The elevated ORP in the stirred mixture indicates a higher level of oxidation, likely driven by the oxidative properties of CaO_2 and LAC. These components contribute to the polymerization of Py, resulting in increased oxidation levels. The process of magnetic stirring likely imparts essential shear forces that promote a microemulsion process, crucial for breaking down larger aggregates into smaller, more uniformly distributed particles. This results in a stable colloidal suspension where the microparticles are evenly dispersed throughout the medium

Further, the spectrometric analysis results depicted in **Fig. 1d** corroborate these observations. The mixture without stirring exhibited reduced absorbance in the range of 400 to 900 nm. Conversely, the stirred LAC-PPy@Car MF formulation displayed a high absorbance across the same spectrum, suggesting polypyrrole formation during oxidative states. This higher absorbance not only confirms the formation of the polymer but also hints at potential applications for NIR-photothermal activities, underscoring its utility for therapeutic strategies where controlled heat generation is advantageous, such as in targeted medical therapies or diagnostics.

The Fourier-transform infrared (FTIR, **Fig. 1e**) spectroscopy analysis of the individual components and the final product, Lac-PPy@Car MF, reveals distinct absorption bands corresponding to various functional groups. The characteristic peaks observed in the FTIR spectra confirm the presence of key functional groups in the materials. For CaO_2, the peaks around 875 cm^{-1} verify the existence of peroxide groups [54]. For LAC, broad absorption bands around 3281 cm^{-1} indicate the presence of hydroxyl (-OH) groups [55]. Carrageenan exhibits a peak at 1241 cm^{-1}, corresponding to the asymmetric stretching of O=S=O [56]. Pyrrole exhibits a characteristic peak attributed to enhanced conjugation. This band observed at 1530 cm^{-1}, shifts upon polymerization, indicating the formation of polypyrrole and the extension of the conjugated system [57]. The appearance of these characteristic bands suggests that the components have chemically interacted to form a stable and integrated lac-PPy@Car MF composite. The X-ray diffraction (XRD, **Fig. 1f**) analysis of Lac-PPy@Car MF reveals distinct peaks at 19.9° and 29°, which are indicative of the potential metal composite's structural characteristics.

The efficacy of the Lac-PPy@Car MF composite in photothermal therapy was assessed by monitoring temperature changes over 5 min under NIR light expo-sure (**Fig. 1g**). The initial temperature of the sample was 24 °C, and the temperature increases approximately to 45°C. The findings confirm that the Lac-PPy@Car MF composite is capable of generating substantial heat upon NIR exposure, making it a promising candidate for therapeutic applications requiring precise thermal control. To further assess the stability and reusability of the Lac-PPy@Car MF composite in photothermal uses, a thermal cycling experiment was conducted **(Fig. S1b)**. This cycling approach aimed to simulate repeated heating and cooling phases, providing insight into the material's ability to maintain consistent photothermal performance. This enhanced photostability ensures reliable long-term performance, making Lac-PPy@Car MF a promising candidate for advanced biomedical applications, including photothermal therapy and thermal-responsive drug delivery systems [58].

Calcein, a fluorochrome, is extensively employed for evaluating cellular viability and mitochondrial activity by fluorescence microscopy [59]. Evaluating cellular viability and the energetic status of mitochondria is crucial. The dye's vibrant fluorescence when exposed to live cells makes it perfect for accurate and immediate cellular imaging. This capability is especially vital in research that necessitates a meticulous examination of mitochondrial dynamics within living cells. Furthermore, the non-toxic properties of calcein guarantee that it does not interfere with cellular metabolism, thereby preserving the integrity of experimental settings.

The Live/Dead assay provided further insights into the biocompatibility of the Lac-PPy@Car MF composite **(Fig. 2a).** The results indicated nearly no dead cells in the control group and with NIR exposure, confirming that the NIR light condition alone induced less cytotoxicity. Similarly, the groups treated with Lac-PPy@Car MF, both with and without NIR exposure, showed fewer to negligible dead cells, demonstrating the non-cytotoxic nature of the composite at the tested concentrations. Fluorescence microscopy revealed a predominance of green-stained live cells across all groups, with minimal red-stained dead cells. This pattern was consistent for the control, NIR-only, and lac-PPy@Car MF-treated groups, indicating that the composite maintains high cell viability and does not induce significant cell death, even when combined with NIR exposure

These findings underscore the excellent biocompatibility of Lac-PPy@Car MF, as evidenced by the lack of dead cells and the abundance of live cells in the assay. The consistent results across different conditions further validate the composite's suitability for biomedical applications, particularly where cell viability is crucial. LAC-PPy@Car MF, when combined with NIR therapy, significantly enhances cell proliferation at a specific concentration, surpassing the proliferation observed at the same concentration without NIR exposure. Moreover, this enhancement is more pronounced compared to samples, both with and without NIR treatment. These findings suggest that NIR-activated LAC-PPy@Car MF may promote fibroblast proliferation, potentially through mechanisms involving mitochondrial activation. The notable phototherapeutic effects of LAC-PPy@Car MF in boosting fibroblast proliferation underscore their potential in regenerative medicine applications. NIR treatment appears to synergize with the microparticles, enhancing cellular functions, possibly by increasing mitochondrial activity, crucial for energy production and cellular growth. This synergistic effect highlights the therapeutic potential of combining LAC-PPy@Car MF with NIR as an innovative approach to enhance cellular regenerative processes.

Fluorescence microscopy studies, as shown in **Fig. 2b**, reveal a stark difference in AhR activation between the control groups and those treated with LAC-PPy@Car MF. Cells in the control group and those

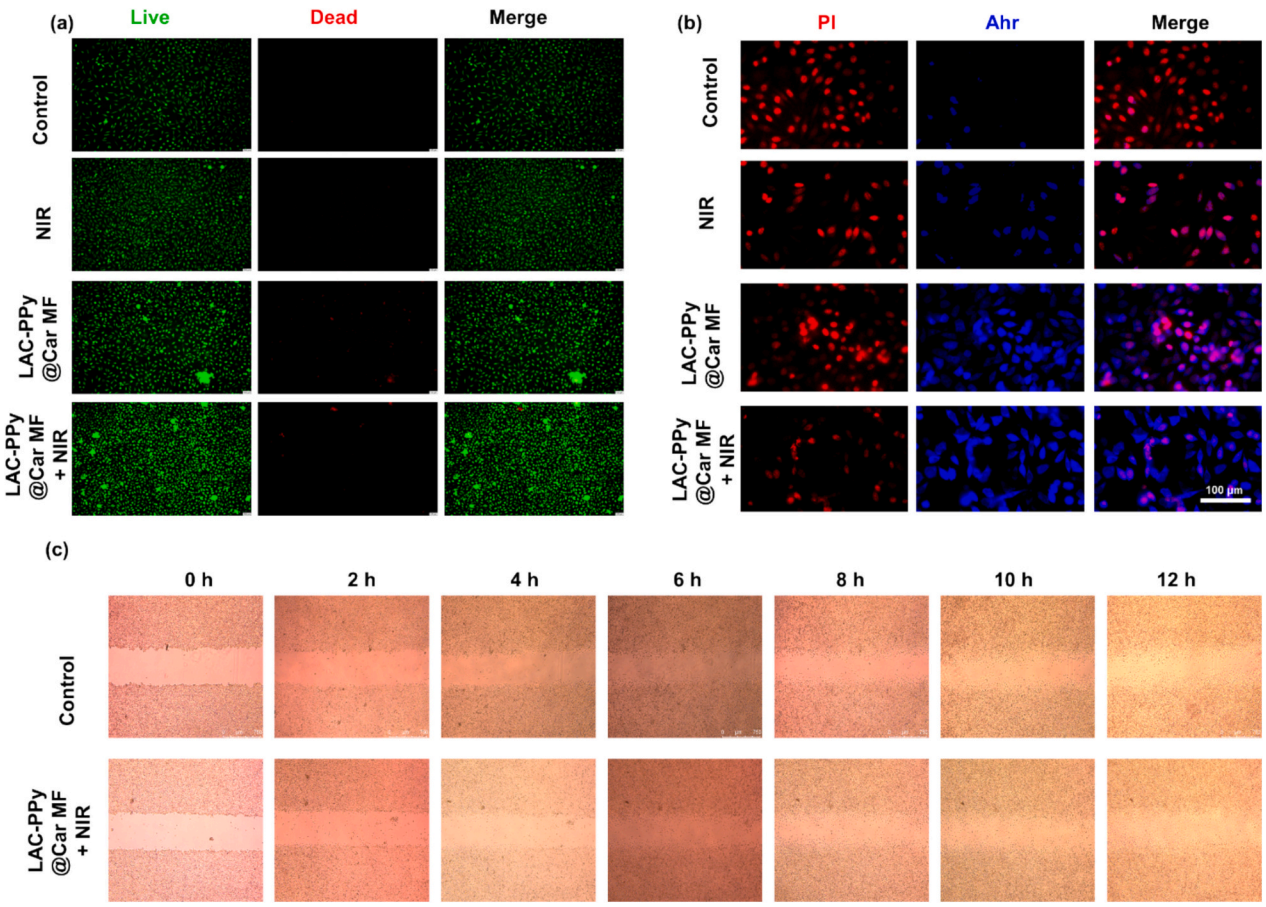

Fig. 2. (a) Live/Dead assay results showing the biocompatibility of LAC-PPy@Car MF under various conditions, including control, NIR-only exposure, and treatment with LAC-PPy@Car MF with and without NIR exposure. Fluorescence microscopy images illustrate a predominance of green-stained live cells with minimal red-stained dead cells, indicating high cell viability and minimal cytotoxicity. (b) Fluorescence microscopy images highlighting Aryl Hydrocarbon receptor (AhR) activation levels in cells treated with LAC-PPy@Car MF, with or without NIR exposure, showing enhanced AhR activity compared to control and NIR-only groups. (c) Cell migration assay tracking the movement of fibroblasts over 12 h under control and LAC-PPy@Car MF-treated conditions with NIR exposure. Time-lapse microscopy images at 0, 2, 4, 6, 8, 10, and 12 h illustrate comparable cellular migration patterns, confirming the non-inhibitory nature of LAC-PPy@Car MF and its potential to support wound healing and tissue regeneration.

exposed solely to NIR exhibited less AhR activity. In contrast, significant activation of AhR was observed in cells treated with LAC-PPy@Car MF, regardless of NIR exposure. This higher expression of AhR aligns with established research linking AhR activation to the biological processing of polycyclic aromatic hydrocarbons (PAHs) [60].

According to prior research, the AhR may enhance cellular proliferation and survival through additional pathways beyond its well-known environmental sensor functions. Specifically, AhR has been implicated in upregulating the L-type amino acid transporter 1 (LAT-1), a key transporter involved in the cellular uptake of amino acids, which are crucial for cellular metabolism and growth [61]. Moreover, AhR is known to stimulate the expression of various growth factors that are directly linked to promoting cell proliferation, highlighting its broader role in cellular development and response mechanisms [62]. Propidium iodide (PI), a DNA-binding fluorescent dye, was used for nuclear staining due to its strong fluorescence upon intercalation with double-stranded nucleic acids. Although PI is commonly used for identifying non-viable cells, in this study, it was employed to visualize nuclei, as it selectively binds DNA once inside the cell [63–66]. This allows for clear nuclear identification, facilitating the assessment of AhR localization and nuclear translocation.

These studies suggest that AhR's involvement extends beyond its traditional role in xenobiotic metabolism, functioning as a significant enhancer of cellular growth and viability. By regulating amino acid transport through LAT-1, AhR ensures that cells have access to essential nutrients necessary for growth and repair, which is particularly crucial in regenerative processes. Furthermore, the ability of AhR to induce growth factors underscores its importance in cellular signaling pathways that lead to proliferation, suggesting that AhR could be a potential target for therapeutic strategies aimed at enhancing tissue regeneration and repair. These multifaceted roles of AhR in cellular physiology affirm its significance beyond its environmental monitoring functions, providing new insights into its contributions to cellular health and potential applications in medical science.

In the cell migration assay (Fig. 2**c**), both the control group and the LAC-PPy@Car MF-treated group with NIR exhibited no visible migration at the initial time point (0 h), suggesting a baseline level of cellular adhesion and minimal spontaneous migration. However, as the assay progressed, with time points at 2 h, 4 h, 6 h, 8 h, 10 h, and 12 h, a noticeable increase in cell migration was observed in both groups. Despite the absence of significant differences in migration patterns between the control and the treated groups at later time points, the gradual increase in migrated cells over time suggests active cellular movement and migration. This observation indicates that the presence of LAC-PPy@Car MF, when combined with NIR exposure, does not inhibit cellular migration but rather allows for a comparable level of migration to that observed in the control group. These findings highlight the biocompatibility and non-inhibitory nature of LAC-PPy@Car MF towards cellular migration, supporting its potential suitability for applications where controlled cellular movement and migration are desired,

such as tissue engineering and wound healing. The absence of any inhibitory effect on cell migration highlights the therapeutic potential of LAC-PPy@Car MF in wound healing applications, underscoring its applicability for therapies aiming at enhancing tissue repair and regeneration.

The study explored the effects of LAC-PPy@Car MF composite in vivo, evaluating its photothermal therapeutic potential, biocompatibility, and impact on tissue regeneration. The experimental design involved three groups: (1) burn injury alone, (2) burn injury + NIR (3) burn injury treated with LAC-PPy@Car MF, and (4) burn injury treated with LAC-PPy@Car MF under NIR exposure. The outcomes were analyzed based on temperature variation and histological changes in soft and skin tissues.

The real-time temperature monitoring (Fig. 3a) demonstrated a distinct increase in local temperature upon NIR exposure in the LAC-PPy@Car MF-treated group compared to the control. The maximum temperature reached ca. nearly 40 °C under NIR light, which is optimal for triggering photothermal effects without causing thermal damage.

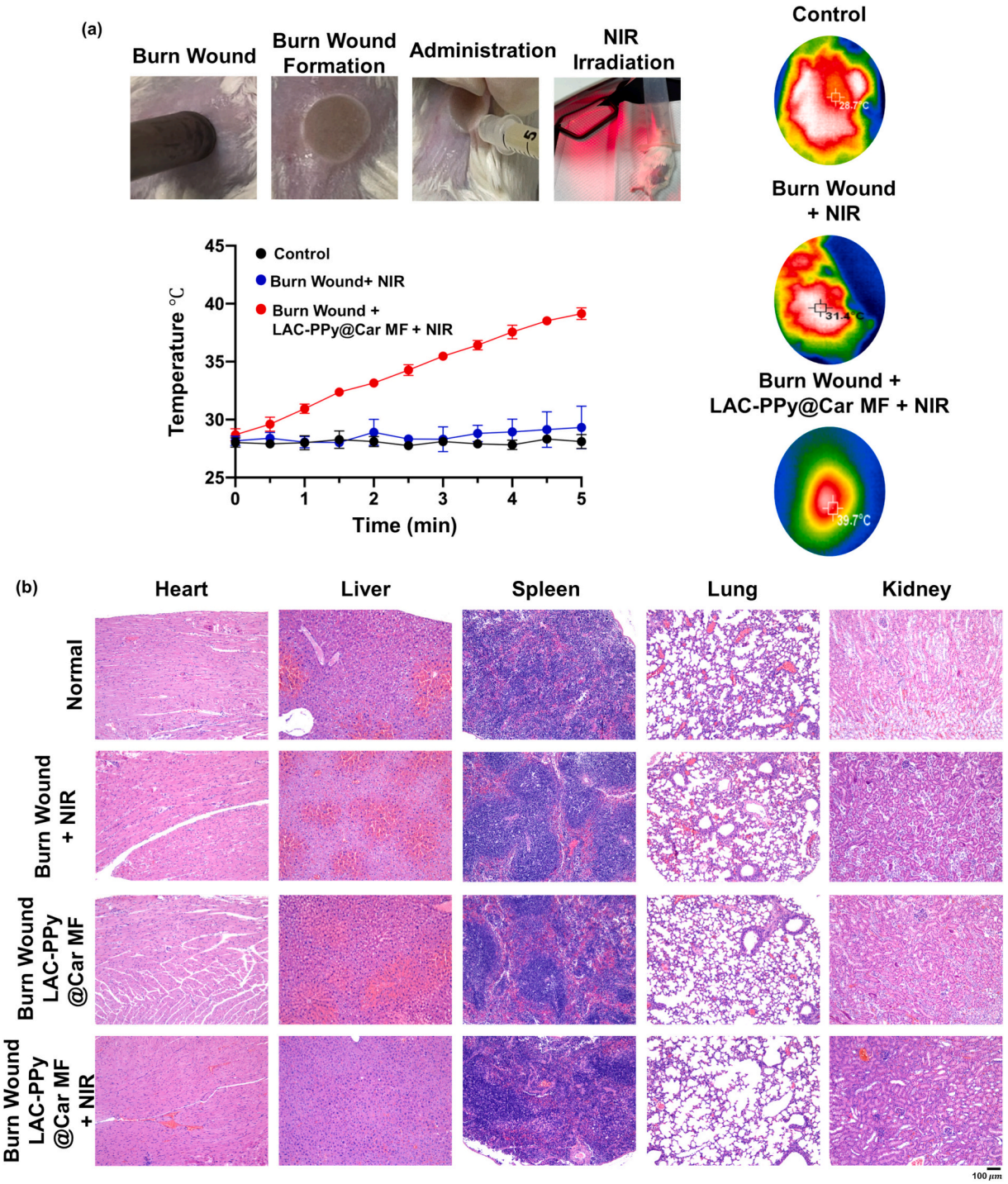

Fig. 3. (a) Representative images and real-time temperature profiles of burn injury sites treated with different formulations: burn wound alone, burn wound + NIR, burn wound + LAC-PPy@Car MF, and burn wound + LAC-PPy@Car MF + NIR. The thermal imaging highlights the localized temperature increase in the NIR-treated group, reaching ca. nearly 40 °C, demonstrating the photothermal effect of the LAC-PPy@Car MF composite. (b) Histological analysis of soft tissues (heart, liver, spleen, lungs, and kidneys) and skin tissues stained with H&E after 14 days.

The burn injury + LAC-PPy@Car MF + NIR group showed a progressive temperature rise over the treatment period, which was higher than the burn injury and burn injury + LAC-PPy@Car MF groups. The wound healing progression over 14 days is illustrated in **Fig. S2.** The wound + NIR, LAC-PPy@Car, both with and without NIR, exhibited wound healing. However, the efficient wound healing was observed in the group of LAC-PPy@Car MF+ NIR, suggesting superior healing efficacy over the 14 days. The control group or wound + NIR group exhibited minimal temperature fluctuations, suggesting that the heating effect was likely attributed to the photothermal properties of PPy. This finding aligns with PPy's well-established ability to absorb NIR light and convert it into heat, leading to hyperthermia, which could stimulate heat shock protein (HSP) expression and protect cells from damage. Moreover, the LAC and Car components contain the nutritional ingredients that are known to promote skin health by mitigating inflammation and enhancing cellular proliferation. The synergy between these components and the photothermal effect of PPy underscores the potential of this composite for non-invasive skin regeneration therapies.

The histological examination of soft tissues, including the heart, liver, spleen, lungs, and kidneys, revealed no significant pathological changes across all treatment groups for 14 days (Fig. 3**b**). This confirms the excellent biocompatibility of the LAC-PPy@Car MF composite, as no toxicological effects were observed. The absence of tissue damage highlights the safety of this formulation for in vivo applications, even under NIR exposure.

The 7-day histological assessment of major organs (heart, liver, spleen, lungs, and kidneys) showed no abnormalities across all groups (Fig. S3), confirming the early biocompatibility of LAC-PPy@Car MF, even with NIR exposure. In skin tissues, the burn injury + LAC-PPy@Car MF + NIR group exhibited early tissue regeneration, with restored epidermal structure and reduced inflammation, resembling normal skin. The burn injury group showed delayed healing, while the burn injury + LAC-PPy@Car MF group demonstrated moderate repair but was less effective than the NIR-treated group. These findings indicate that LAC-PPy@Car MF, especially with NIR activation, enhances early wound healing, reinforcing its safety and regenerative potential.

LAC and Car, as bioactive materials, provided additional benefits by enhancing skin hydration, reducing inflammation, and supporting cellular adhesion and proliferation. These properties, combined with the localized heat generation from NIR exposure, created an optimal microenvironment for wound healing and tissue regeneration. The results of this study highlight the promising potential of LAC-PPy@Car MF as a safe and effective therapeutic agent for skin regeneration. The composite demonstrated excellent biocompatibility, significant photothermal effects under NIR exposure, and accelerated wound healing through synergistic mechanisms involving cellular protection, proliferation, and anti-inflammatory effects. Future investigations could focus on optimizing the dosage and exploring the long-term efficacy of this composite in various regenerative medicine applications.

The immunofluorescence staining (Fig. 4**a**) for AhR (blue fluorescence) in skin tissues provides critical insights into the biological effects of LAC-PPy@Car MF and NIR exposure. The normal skin group showed minimal AhR expression, indicative of baseline cellular activity. In contrast, the burn wound group exhibited a slight increase in AhR activity. The immunofluorescence staining for AhR in skin tissues at 7 days showed a stronger fluorescence intensity. The normal skin group showed minimal AhR expression, while the burn wound group exhibited a slight increase. The burn wound + LAC-PPy@Car MF group demonstrated a notable upregulation of AhR expression, further enhanced in the burn injury + LAC-PPy@Car MF + NIR group, where AhR levels peaked. The higher fluorescence intensity at 7 days suggests an earlier and more pronounced activation of AhR, likely reflecting the role of LAC-PPy@Car MF + NIR in stimulating protective cellular responses, reducing oxidative stress, and promoting tissue regeneration.

Interestingly, in the 14 days, the burn wound+ LAC-PPy@Car MF groups displayed a tendency in reduction of AhR expression. AhR expression may decrease over time. AhR is known to regulate cellular responses to oxidative stress and promote cellular proliferation and survival by modulating pathways such as amino acid transport and growth factor expression. The observed activation of AhR supports the hypothesis that LAC-PPy@Car MF, particularly under NIR exposure, could enhance cellular protective mechanisms, reduce inflammation, and stimulate regenerative processes. These findings highlight the composite's potential for skin repair and therapeutic applications.

The EDU staining (green fluorescence) results provide a direct assessment of cellular proliferation in response to different treatments (Fig. 4**b**). At 7 days, the normal skin group exhibited baseline cellular proliferation, while the burn injury group showed significantly reduced proliferation. The burn wound + LAC-PPy@Car MF group demonstrated a notable increase in proliferation compared to the burn injury group, highlighting the early regenerative potential of the composite. This effect was even more pronounced in the burn wound + LAC-PPy@Car MF + NIR group, which exhibited the highest fluorescence intensity, suggesting enhanced cellular proliferation and accelerated tissue repair. By 14 days, the normal skin group maintained baseline proliferation, while the burn wound group continued to show reduced proliferation. The burn wound + LAC-PPy@Car MF group exhibited a sustained high proliferation compared to the untreated burn group, reinforcing its role in promoting tissue regeneration. The burn wound + LAC-PPy@Car MF + NIR group continued to show the highest proliferation levels among all groups, confirming the long-term benefits of NIR-induced photothermal therapy. However, fluorescence intensity was stronger at 7 days than at 14 days, indicating that cellular proliferation and metabolic activity peak earlier in the healing process, likely due to enhanced mitochondrial function, ATP production, and metabolic activation stimulated by NIR exposure. These results suggest that the synergistic effect of LAC-PPy@Car MF and NIR is most effective in the early stages of tissue repair, with a progressive decline in proliferation as tissue maturation advances by 14 days.

This study offers promising insights into the potential applications of LAC-PPy@Car MF in regenerative medicine, particularly for skin repair and wound healing. Future studies could further elucidate the molecular mechanisms underlying these effects, optimize the composite's formulation, and explore its efficacy in other therapeutic contexts, such as chronic wounds and inflammatory skin disorders. The results from Fig. 4 highlight the remarkable therapeutic potential of the LAC-PPy@Car MF composite. By leveraging AhR activation and enhanced cellular proliferation, particularly under NIR exposure, this composite represents a highly promising approach for accelerating tissue regeneration and improving skin health. These findings pave the way for further exploration of its applications in regenerative medicine and photothermal therapies.

The activation of the AhR in the burn injury + LAC-PPy@Car MF + NIR group highlights its crucial role in the observed potentially connecting to regenerative effects. AhR activation is known to modulate anti-inflammatory pathways, enhance cellular survival, and promote tissue remodeling, all of which contribute to accelerated wound healing [67]. The dual effect of MF and NIR exposure stimulates AhR activity and AhR signaling mediates oxidative stress and has a role in keratinocyte development, skin barrier function, and skin pigmentation in healthy skin [68–70].

The expression of protective heat shock proteins (HSP, green fluorescence) was evaluated to determine the cellular response to thermal stress and photothermal therapy (Fig. 5**a**). The normal skin group exhibited baseline levels of HSP expression, while the burn injury group showed a slight increase, likely as a response to thermal injury. The HSPs further support this process by protecting cells from oxidative stress and improving their metabolic function [71]. Heat shock proteins (HSPs) play a vital role in skin protection and repair by acting as molecular chaperones, ensuring proper protein folding and stability under stress. In the epidermis, HSPs support cell differentiation and protect against UV-induced damage. HSP27, a marker of epidermal differentiation,

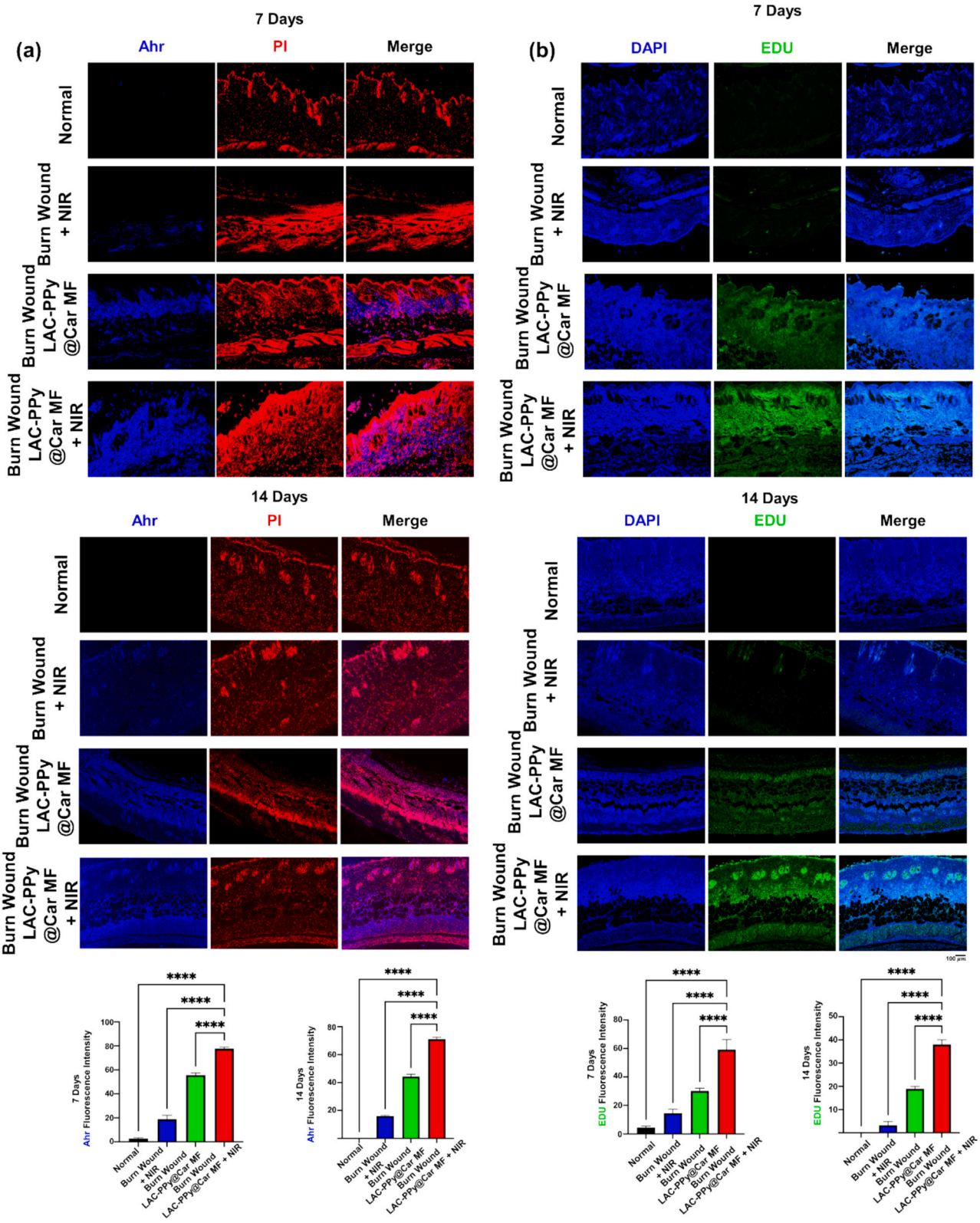

Fig. 4. (a) Immunofluorescence staining of aryl hydrocarbon receptor (AhR, blue fluorescence) in skin tissues from four groups for 7 days and 14 days: normal skin, burn wound, burn wound + NIR, burn wound + LAC-PPy@Car MF, and burn wound + LAC-PPy@Car MF + NIR. (b) EDU staining (green fluorescence) for cellular proliferation across the same groups for 7 days and 14 days. The burn wound + LAC-PPy@Car MF group showed improved proliferation, while the burn wound + LAC-PPy@Car MF + NIR group demonstrated the highest level of cellular proliferation, indicating accelerated tissue regeneration. Quantitative analysis reveals a significant increase in both AhR activation and cellular proliferation in the burn injury + LAC-PPy@Car MF + NIR-treated group compared to all other groups. These results underscore the composite's potential for promoting skin regeneration and wound healing through AhR activation and enhanced cellular proliferation. The difference of $P \leq 0.05$ is considered statistically significant. Statistically significant differences were considered for $^{*}p \leq 0.05$, $^{**}p \leq 0.01$, $^{***}p \leq 0.001$ and $^{****}p \leq 0.0001$.

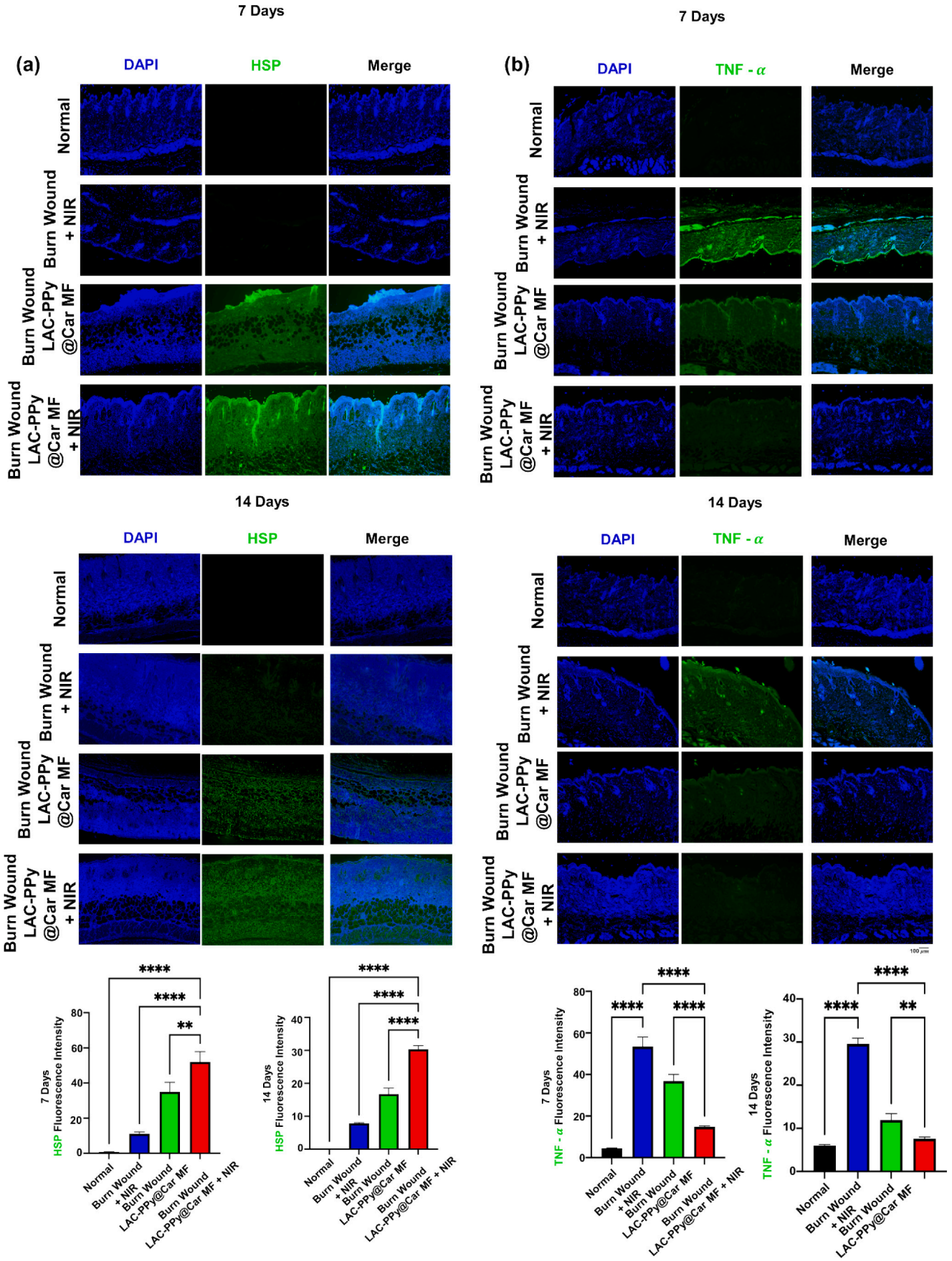

(caption on next page)

Fig. 5. (a) Immunofluorescence staining for heat shock protein (HSP, green fluorescence) expression in the same groups (normal, burn wound + NIR, burn wound + LAC-PPy@Car MF, burn wound + LAC-PPy@Car MF + NIR). The burn wound + LAC-PPy@Car MF + NIR group demonstrated the highest HSP expression, indicating enhanced cellular protection and repair. Quantitative analysis reveals a significant reduction in oxidative stress and upregulation of HSP in the NIR-treated group compared to all other groups. (b) Immunofluorescence staining of TNF-α (green fluorescence) in skin tissues from four groups: Normal skin, burn wound + NIR, burn wound + LAC-PPy@Car MF, and burn wound + LAC-PPy@Car MF + NIR. The burn wound + LAC-PPy@Car MF + NIR group showed the most significant reduction in oxidative stress, approaching levels observed in the normal skin group. These results underscore the composite's potential for reducing oxidative damage and promoting tissue regeneration. The difference of $P \leq 0.05$ is considered statistically significant. Statistically significant differences were considered for $^{*}p \leq 0.05$, $^{**}p \leq 0.01$, $^{***}p \leq 0.001$ and $^{****}p \leq 0.0001$.

increases with keratinocyte maturation and is linked to age-related skin changes. Since HSPs can be modulated pharmacologically, they hold the potential for developing topical and systemic treatments to prevent skin damage, improve resilience, and address keratinocyte disorders [72]. These findings suggest that AhR activation, in combination with photothermal therapy, plays a pivotal role in optimizing the wound healing microenvironment, making LAC-PPy@Car MF a promising candidate for advanced skin regeneration therapies.

In the immunofluorescence staining for HSP in skin tissues at 7 days, the normal skin group exhibited minimal HSP expression, while the burn injury group showed a moderate increase, indicating a stress-induced cellular response. The burn wound + LAC-PPy@Car MF group demonstrated an upregulation of HSP expression, with the highest fluorescence intensity observed in the burn wound + LAC-PPy@Car MF + NIR group. The elevated HSP levels at 7 days suggest a strong heat shock response, contributing to protein stabilization, cellular protection, and enhanced tissue recovery, highlighting the early therapeutic potential of LAC-PPy@Car MF + NIR in accelerating wound healing. By 14 days, HSP expression remained upregulated in the burn wound + LAC-PPy@Car MF group, showing continued activation of protective cellular mechanisms. However, fluorescence intensity at 14 days was lower than at 7 days, suggesting that the heat shock response peaks earlier in the healing process and gradually declines as tissue recovery progresses. The burn wound + LAC-PPy@Car MF + NIR group continued to exhibit the highest HSP expression at 14 days compared to other groups, emphasizing the synergistic effect of NIR-induced photothermal therapy and bioactive components in promoting sustained cellular protection and wound repair. The stronger fluorescence at 7 days compared to 14 days reinforces the early, intense activation of the heat shock response, which diminishes over time as tissue healing advances. HSPs are known to play a crucial role in cellular homeostasis by protecting cells from thermal and oxidative stress, stabilizing unfolded proteins, and facilitating cellular repair processes. The elevated HSP levels observed in the NIR-treated group suggest that the composite creates an optimal microenvironment for accelerated tissue repair and regeneration, leveraging both thermal and bioactive stimuli.

TNF-α plays a vital role in wound healing by supporting immune defense, immune cell recruitment, fibroblast proliferation, keratinocyte activation, and growth factor regulation. While it is beneficial in the early phases of healing, an overproduction or prolonged inflammatory response may cause complications such as excessive scarring or tissue obstruction, ultimately hindering the healing process. The wound healing effects of LAC-PPy@Car MF + NIR were assessed by measuring TNF-α at 7 and 14 days across burn wound + NIR, burn wound + LAC-PPy@Car MF + NIR, and normal tissue groups (**Fig. 5b**). The burn wound + NIR group exhibited the highest TNF-α level, indicating prolonged inflammation, while the burn wound + LAC-PPy@Car MF + NIR group showed a significant reduction, suggesting enhanced healing. By 14 days, TNF -α in the burn wound + LAC-PPy@Car MF + NIR group approached those of the normal tissue group, confirming the composite's anti-inflammatory and wound-healing potential. These findings highlight the effectiveness of LAC-PPy@Car MF with NIR irradiation in modulating inflammation and accelerating tissue regeneration. During the proliferation phase of wound healing, macrophage-derived TNF-α plays a crucial role in extracellular matrix (ECM) formation by stimulating fibroblasts to produce proteoglycans and fibronectin.

4. Conclusion

This study highlights the promising potential of LAC-PPy@Car MF as a biocompatible and effective composite for regenerative medicine applications. The Live/Dead assay confirmed its non-cytotoxic nature, with high cell viability observed across all conditions. Notably, the combination of LAC-PPy@Car MF with NIR exposure possesses the potential for skin tissue engineering. Additionally, microscopic data revealed increased AhR activation in treated groups, suggesting a role in cellular biological effects. The in vivo findings further validated the LAC-PPy@Car MF composite's therapeutic potential. Histological analysis confirmed excellent biocompatibility, with no adverse effects on major organs. The burn injury model demonstrated wound healing in the LAC-PPy@Car MF + NIR group, attributed to mechanisms involving AhR activation, heat shock protein expression, and anti-inflammatory properties of phototherapeutic LAC-PPy@Car MF.

Overall, this study establishes phototherapeutic LAC-PPy@Car MF as an effective as well as safe biomaterial for skin tissue engineering. Its ability to enhance tissue repair, particularly under NIR exposure, makes it a promising candidate for future applications in wound healing and regenerative medicine. Further research should focus on optimizing its dosage and evaluating its long-term biosafety and therapeutic efficacy.

CRediT authorship contribution statement

Sih-Chi Chuang: Conceptualization, Data curation, Methodology, Writing – original draft, Writing – review & editing. **Shih-An Yu:** Conceptualization, Data curation, Methodology, Writing – original draft, Writing – review & editing. **Pei-Chia Hung:** Data curation, Methodology, Formal analysis, Writing – original draft, Writing – review & editing. **Andrew E.-Y. Chuang:** Conceptualization, Data curation, Methodology, Formal analysis, Funding acquisition, Investigation, Project administration, Resources, Supervision, Validation, Software Visualization, Writing – original draft, Writing – review & editing. **Jia-Wei Liang:** Data curation, Methodology, Formal analysis, Writing – original draft, Writing – review & editing. **Lekshmi Rethi:** Data curation, Methodology, Formal analysis, Writing – original draft, Writing – review & editing. **Chih-Kuang Chen:** Writing – review & editing. **Hsu-Wei Fang:** Writing – review & editing. **Hieu Trung Nguyen:** Writing – review & editing. **Hsien-Tsung Lu:** Conceptualization, Data curation, Methodology, Formal analysis, Funding acquisition, Investigation, Project administration, Resources, Supervision, Validation, Software Visualization, Writing – original draft, Writing – review & editing..

Consent for publication

All of the authors involved in this study have agreed to the publication of this manuscript.

Declaration of competing interest

The authors declare that there are no conflicts of interest.

Acknowledgments

This study was financially supported by grants from the National Science and Technology Council (NSTC), Taiwan [grant numbers 112-

2221-E-038-002 -MY3, and 112-2622-E-038-006-].

Appendix A. Supplementary data

Supplementary data to this article can be found online at https://doi.org/10.1016/j.ijbiomac.2025.144436.

Data availability

Data will be made available on request.

References

[1] G.C. Gurtner, S. Werner, Y. Barrandon, M.T. Longaker, Wound repair and regeneration, J. Nature 453 (7193) (2008) 314–321, https://doi.org/10.1038/nature07039.

[2] E.M. Tottoli, R. Dorati, I. Genta, E. Chiesa, S. Pisani, B. Conti, Skin wound healing process and new emerging technologies for skin wound care and regeneration, Pharmaceutics 12 (8) (2020) 735.

[3] Broughton, G., Janis, J. AC wound healing: an overview. J. Plast. Reconstr. Surg. 117(7 Suppl).

[4] P.S. Murphy, G.R. Evans, Advances in wound healing: a review of current wound healing products, J. Plast. Surg. Int. (2012) (2012).

[5] S. Mascharak, H.E. des Jardins-Park, M.F. Davitt, M. Griffin, M.R. Borrelli, A. L. Moore, K. Chen, B. Duoto, M. Chinta, D.S. Foster, A.H. Shen, M. Januszyk, S. H. Kwon, G. Wernig, D.C. Wan, H.P. Lorenz, G.C. Gurtner, M.T. Longaker, Preventing Engrailed-1 activation in fibroblasts yields wound regeneration without scarring, Science (New York, N.Y.) 372 (6540) (2021).

[6] Y. Li, X. He, R. Kawaguchi, Y. Zhang, Q. Wang, A. Monavarfeshani, Z. Yang, B. Chen, Z. Shi, H. Meng, S. Zhou, J. Zhu, A. Jacobi, V. Swarup, P.G. Popovich, D. H. Geschwind, Z. He, Microglia-organized scar-free spinal cord repair in neonatal mice, Nature 587 (7835) (2020) 613–618.

[7] L. Zhou, H. Zheng, Z. Liu, S. Wang, Z. Liu, F. Chen, H. Zhang, J. Kong, F. Zhou, Q. Zhang, Conductive antibacterial hemostatic multifunctional scaffolds based on Ti(3)C(2)T(x) MXene Nanosheets for promoting multidrug-resistant Bacteria-infected wound healing, ACS Nano 15 (2) (2021) 2468–2480.

[8] B.A. Shook, R.R. Wasko, G.C. Rivera-Gonzalez, E. Salazar-Gatzimas, F. López-Giráldez, B.C. Dash, A.R. Muñoz-Rojas, K.D. Aultman, R.K. Zwick, V. Lei, J. L. Arbiser, K. Miller-Jensen, D.A. Clark, H.C. Hsia, V. Horsley, Myofibroblast proliferation and heterogeneity are supported by macrophages during skin repair, Science (New York, N.Y.) 362 (6417) (2018) eaar2971, https://doi.org/10.1126/science.aar2971.

[9] Z. Yang, D. Gao, X. Guo, L. Jin, J. Zheng, Y. Wang, S. Chen, X. Zheng, L. Zeng, M. Guo, X. Zhang, Z. Tian, Fighting immune cold and reprogramming immunosuppressive tumor microenvironment with red blood cell membrane-camouflaged Nanobullets, ACS Nano 14 (12) (2020) 17442–17457.

[10] C. Kalirajan, T. Palanisamy, Bioengineered hybrid collagen scaffold tethered with silver-Catechin nanocomposite modulates angiogenesis and TGF-β toward Scarless healing in chronic deep second degree infected burns, Adv. Healthc. Mater. 9 (12) (2020) e2000247.

[11] Y. Wang, Y. Wu, L. Long, L. Yang, D. Fu, C. Hu, Q. Kong, Y. Wang, Inflammation-responsive drug-loaded hydrogels with sequential hemostasis, antibacterial, and anti-inflammatory behavior for chronically infected diabetic wound treatment, ACS Appl. Mater. Interfaces 13 (28) (2021) 33584–33599.

[12] Y. Shen, G. Xu, H. Huang, K. Wang, H. Wang, M. Lang, H. Gao, S. Zhao, Sequential release of small extracellular vesicles from Bilayered Thiolated alginate/polyethylene glycol Diacrylate hydrogels for Scarless wound healing, ACS Nano 15 (4) (2021) 6352–6368.

[13] D. Khodabakhshi, A. Eskandarinia, A. Kefayat, M. Rafienia, S. Navid, S. Karbasi, J. Moshtaghian, In vitro and in vivo performance of a propolis-coated polyurethane wound dressing with high porosity and antibacterial efficacy, J Colloids surfaces B: Biointerfaces 178 (2019) 177–184.

[14] T. Tokatlian, C. Cam, T. Segura, Porous hyaluronic acid hydrogels for localized nonviral DNA delivery in a diabetic wound healing model, J Advanced healthcare materials 4 (7) (2015) 1084–1091.

[15] X. Zhao, H. Wu, B. Guo, R. Dong, Y. Qiu, P. Ma, Antibacterial anti-oxidant electroactive injectable hydrogel as self-healing wound dressing with hemostasis and adhesiveness for cutaneous wound healing, Biomaterials 122 (2017) 34–47.

[16] Y. Yang, X. Zhao, J. Yu, X. Chen, R. Wang, M. Zhang, Q. Zhang, Y. Zhang, S. Wang, Y. Cheng, Bioactive skin-mimicking hydrogel band-aids for diabetic wound healing and infectious skin incision treatment, J Bioactive materials 6 (11) (2021) 3962–3975.

[17] J. Miao, R.C. Pangule, E.E. Paskaleva, E.E. Hwang, R.S. Kane, R.J. Linhardt, J. S. Dordick, Lysostaphin-functionalized cellulose fibers with antistaphylococcal activity for wound healing applications, Biomaterials 32 (36) (2011) 9557–9567.

[18] Y. Li, J. Wang, Y. Wang, W. Cui, Advanced electrospun hydrogel fibers for wound healing, Compos. Part B Eng. 223 (2021) 109101.

[19] H. Xu, F. Lv, Y. Zhang, Z. Yi, Q. Ke, C. Wu, M. Liu, J. Chang, Hierarchically micro-patterned nanofibrous scaffolds with a nanosized bio-glass surface for accelerating wound healing, Nanoscale 7 (44) (2015) 18446–18452.

[20] M. Liu, X.-P. Duan, Y.-M. Li, D.-P. Yang, Y.-Z. Long, Electrospun nanofibers for wound healing, Mater. Sci. Eng. C 76 (2017) 1413–1423.

[21] B. Yu, C. He, W. Wang, Y. Ren, J. Yang, S. Guo, Y. Zheng, X. Shi, Asymmetric wettable composite wound dressing prepared by electrospinning with bioinspired micropatterning enhances diabetic wound healing, ACS Appl. Bio Mater. 3 (8) (2020) 5383–5394.

[22] L. Chen, S. Wang, Q. Yu, P.D. Topham, C. Chen, L. Wang, A comprehensive review of electrospinning block copolymers, J Soft Matter 15 (12) (2019) 2490–2510.

[23] G. Han, R. Ceilley, Chronic wound healing: a review of current management and treatments, Adv. Ther. 34 (2017) 599–610.

[24] B. Azimi, H. Maleki, L. Zavagna, J.G. De la Ossa, S. Linari, A. Lazzeri, S. Danti, Bio-based electrospun fibers for wound healing, Journal of functional biomaterials 11 (3) (2020) 67, https://doi.org/10.3390/jfb11030067.

[25] H.A. Rather, R. Thakore, R. Singh, D. Jhala, S. Singh, R. Vasita, Antioxidative study of cerium oxide nanoparticle functionalised PCL-gelatin electrospun fibers for wound healing application, Bioactive materials 3 (2) (2018) 201–211.

[26] H. Fan, R. Ding, W. Liu, X. Zhang, R. Li, B. Wei, S. Su, F. Jin, C. Wei, X. He, X. Li, C. Duan, Heat shock protein 22 modulates NRF1/TFAM-dependent mitochondrial biogenesis and DRP1-sparked mitochondrial apoptosis through AMPK-PGC1α signaling pathway to alleviate the early brain injury of subarachnoid hemorrhage in rats, Redox Biol. 40 (2021) 101856.

[27] A. Jeuken, B.J. Keser, E. Khan, A. Brouwer, J. Koeman, M.S. Denison, Activation of the ah receptor by extracts of dietary herbal supplements, vegetables, and fruits, J. Agric. Food Chem. 51 (18) (2003) 5478–5487.

[28] N. Barouti, C. Mainetti, L. Fontao, O. Sorg, L-tryptophan as a novel potential pharmacological treatment for wound healing via aryl hydrocarbon receptor activation, Dermatology (Basel, Switzerland) 230 (4) (2015) 332–339.

[29] J. Cao, W. Zhu, A.-G. Shen, J.-M. Hu, Rational synthesis of three-layered plasmonic nanocomposites of copper sulfide/gold/zinc-doped Prussian blue analogues for improved photothermal disinfection and wound healing, J. Colloid Interface Sci. 610 (2022) 621–633.

[30] S. Yu, G. Li, P. Zhao, Q. Cheng, Q. He, D. Ma, W. Xue, NIR-laser-controlled hydrogen-releasing PdH nanohydride for synergistic hydrogen-photothermal antibacterial and wound-healing therapies, Adv. Funct. Mater. 29 (50) (2019) 1905697.

[31] L. Chen, Q. Yu, K. Cheng, P.D. Topham, M. Xu, X. Sun, Y. Pan, Y. Jia, S. Wang, L. Wang, Can photothermal post-operative cancer treatment be induced by a thermal trigger? ACS Appl. Mater. Interfaces 13 (51) (2021) 60837–60851.

[32] Q. Xin, H. Shah, A. Nawaz, W. Xie, M.Z. Akram, A. Batool, L. Tian, S.U. Jan, R. Boddula, B. Guo, Antibacterial carbon-based nanomaterials, Adv. Mater. 31 (45) (2019) 1804838.

[33] Y. Feng, J. Qin, Y. Zhou, Q. Yue, J.J.J.o.C. Wei, I. Science, Spherical mesoporous Fe-NC single-atom nanozyme for photothermal and catalytic synergistic antibacterial therapy, Journal of Colloid Interface Science 606 (2022) 826–836.

[34] C.-H. Liu, P.-R. Jheng, L. Rethi, C. Godugu, C.Y. Lee, Y.-T. Chen, H.T. Nguyen, E.-Y. Chuang, P-selectin mediates targeting of a self-assembling phototherapeutic nanovehicle enclosing dipyridamole for managing thromboses, J. Nanobiotechnol. 21 (1) (2023) 260.

[35] K.T. Liu, E.D. Quiñones, M.H. Liu, C.W. Lin, Y.T. Chen, C.C. Chiang, K.C.W. Wu, Y. J. Fan, E.Y. Chuang, J. Yu, A biomimicking and multiarm self-indicating nanoassembly for site-specific photothermal-potentiated thrombolysis assessed in microfluidic and in vivo models, Adv. Healthc. Mater. 12 (24) (2023) 2300682.

[36] L. Rethi, C. Mutalik, L. Rethi, W.-H. Chiang, H.-L. Lee, W.-Y. Pan, T.-S. Yang, J.-F. Chiou, Y.-J. Chen, E.-Y. Chuang, Lu Long Sheng, Molecularly targeted photothermal ablation of epidermal growth factor receptor-expressing cancer cells with a polypyrrole–iron oxide–afatinib nanocomposite, Cancers 14 (20) (2022) 5043.

[37] E.D. Quiñones, T.-Y. Lu, K.-T. Liu, Y.-J. Fan, E.-Y. Chuang, J. Yu, Glycol chitosan/iron oxide/polypyrrole nanoclusters for precise chemodynamic/photothermal synergistic therapy, Int. J. Biol. Macromol. 203 (2022) 268–279.

[38] Y. Wang, Z. Wang, W. Guo, L. Bai, Q. Luo, C. Kwong Cheng, W. Zhang, D. Wu, C. Hu, Y. Wang, An injectable extracellular matrix-mimicking conductive hydrogel for sequential treatment of ischemic stroke, Chem. Eng. J. 502 (2024) 158039.

[39] X. Ren, Y. Han, J. Wang, Y. Jiang, Z. Yi, H. Xu, Q. Ke, An aligned porous electrospun fibrous membrane with controlled drug delivery–an efficient strategy to accelerate diabetic wound healing with improved angiogenesis, Acta Biomater. 70 (2018) 140–153.

[40] L. Wang, L. Mao, F. Qi, X. Li, M.W. Ullah, M. Zhao, Z. Shi, G. Yang, Synergistic effect of highly aligned bacterial cellulose/gelatin membranes and electrical stimulation on directional cell migration for accelerated wound healing, Chem. Eng. J. 424 (2021) 130563.

[41] Q. Zhao, J. Wang, Y. Wang, H. Cui, X. Du, A stage-specific cell-manipulation platform for inducing endothelialization on demand, Natl. Sci. Rev. 7 (3) (2020) 629–643.

[42] Y. Wu, C. Chen, Y. Jia, J. Wu, Y. Huang, L. Wang, Review on electrospun ultrafine phase change fibers (PCFs) for thermal energy storage, Appl. Energy 210 (2018) 167–181.

[43] T. Wu, H. Li, J. Xue, X. Mo, Y. Xia, Photothermal welding, melting, and patterned expansion of nonwoven mats of polymer nanofibers for biomedical and printing applications, Angew. Chem. Int. Ed. 58 (46) (2019) 16416–16421.

[44] A. P, A. P, R.J. M, J.M. Joy, S. Mathew, Developmental prospects of carrageenan-based wound dressing films: unveiling techno-functional properties and freeze-drying technology for the development of absorbent films - a review, Int. J. Biol. Macromol. 276 (Pt 1) (2024) 133668, https://doi.org/10.1016/j.ijbiomac.2024.133668.

[45] W. Zhao, X. Yang, L. Li, Soy protein-based wound dressings: a review of their preparation, properties, and perspectives, ACS Appl. Mater. Interfaces 16 (31) (2024) 40356–40370.

[46] C.C. Yang, M.S. Wu, H. Hsu, Management of diabetic foot ulcers using topical probiotics in a soybean-based concentrate: a multicentre study, J. Wound Care 32 (Sup12) (2023) S16–s21.
[47] C.-S. Yeh, R. Wang, W.-C. Chang, Y.-h. Shih, Synthesis and characterization of stabilized oxygen-releasing CaO2 nanoparticles for bioremediation, J. Environ. Manag. 212 (2018) 17–22.
[48] D. Horák, Effect of reaction parameters on the particle size in the dispersion polymerization of 2-hydroxyethyl methacrylate, J. Polym. Sci. A Polym. Chem. 37 (20) (1999) 3785–3792.
[49] D. Horák, N. Semenyuk, F. Lednický, Effect of the reaction parameters on the particle size in the dispersion polymerization of 2-hydroxyethyl and glycidyl methacrylate in the presence of a ferrofluid, J. Polym. Sci. A Polym. Chem. 41 (2003) 1848–1863.
[50] Y. Tan, K. Ghandi, Kinetics and mechanism of pyrrole chemical polymerization, Synth. Met. 175 (2013) 183–191.
[51] P. Kaewdee, N. Chandet, G. Rujijanagul, C. Randorn, Multicatalytic properties of nanoparticle CaO2 synthesized by a novel, simple and economical method for wastewater treatment, Catal. Commun. 84 (2016) 151–154.
[52] R. Patil, T. Speaker, Carrageenan as an anionic polymer for aqueous microencapsulation, Drug Deliv. 5 (3) (1998) 179–182.
[53] R. Holze, Overoxidation of intrinsically conducting polymers, Polymers 14 (8) (2022) 1584.
[54] M. Zhang, R. Song, Y. Liu, Z. Yi, X. Meng, J. Zhang, Z. Tang, Z. Yao, Y. Liu, X. Liu, W. Bu, Calcium-overload-mediated tumor therapy by calcium peroxide nanoparticles, Chem 5 (8) (2019) 2171–2182.
[55] N.K. Mohammed, A.M. Alhelli, A.S. Meor Hussin, Influence of different combinations of wall materials on encapsulation of oil by spray dryer, J. Food Process Eng. 44 (3) (2021) e13639.
[56] W.A.K. Mahmood, M.M. Rahman Khan, C.Y. Teow, Effects of reaction temperature on the synthesis and thermal properties of carrageenan ester, J. Phys. Sci. 25 (2014) 123–138.
[57] O.U. Izevbekhai, W.M. Gitari, N.T. Tavengwa, W.B. Ayinde, R. Mudzielwana, Response surface optimization of oil removal using synthesized Polypyrrole-silica polymer composite, Molecules 25 (20) (2020) 4628.
[58] Z. Zha, X. Yue, Q. Ren, Z. Dai, Uniform Polypyrrole nanoparticles with high Photothermal conversion efficiency for Photothermal ablation of Cancer cells, Adv. Mater. 25 (5) (2013) 777–782.
[59] C. Beghetto, C. Renken, O. Eriksson, G. Jori, P. Bernardi, F. Ricchelli, Implications of the generation of reactive oxygen species by photoactivated calcein for mitochondrial studies, Eur. J. Biochem. 267 (17) (2000) 5585–5592.
[60] J. Vondráček, K. Pěnčíková, J. Neča, M. Ciganek, A. Grycová, Z. Dvořák, M. Machala, Assessment of the aryl hydrocarbon receptor-mediated activities of polycyclic aromatic hydrocarbons in a human cell-based reporter gene assay, Environ. Pollut. 220 (2017) 307–316.
[61] J. Yin, B. Sheng, Y. Qiu, K. Yang, W. Xiao, H. Yang, Role of AhR in positive regulation of cell proliferation and survival, Cell Prolif. 49 (5) (2016) 554–560.
[62] M. Karasová, J. Procházková, Z. Tylichová, R. Fedr, M. Ciganek, M. Machala, Z. Dvořák, B. Vyhlídalová, I. Zůvalová, J. Ehrmann, Inhibition of aryl hydrocarbon receptor (AhR) expression disrupts cell proliferation and alters energy metabolism and fatty acid synthesis in colon cancer cells, Cancers 14 (17) (2022) 4245.
[63] L.C. Crowley, A.P. Scott, B.J. Marfell, J.A. Boughaba, G. Chojnowski, N. J. Waterhouse, Measuring cell death by Propidium iodide uptake and flow cytometry, Cold Spring Harb Protoc 2016 (7) (2016).
[64] C. Riccardi, I. Nicoletti, Analysis of apoptosis by propidium iodide staining and flow cytometry, Nat. Protoc. 1 (3) (2006) 1458–1461.
[65] A.D. Deitch, H. Law, R. deVere White, A stable propidium iodide staining procedure for flow cytometry, J. Histochem. Cytochem. 30 (9) (1982) 967–972.
[66] T. Crompton, M.C. Peitsch, H.R. MacDonald, J. Tschopp, Propidium iodide staining correlates with the extent of DNA degradation in isolated nuclei, Biochem. Biophys. Res. Commun. 183 (2) (1992) 532–537.
[67] N.C. Sondermann, S. Faßbender, F. Hartung, A.M. Hätälä, K.M. Rolfes, C.F. A. Vogel, T. Haarmann-Stemmann, Functions of the aryl hydrocarbon receptor (AHR) beyond the canonical AHR/ARNT signaling pathway, Biochem. Pharmacol. 208 (2023) 115371.
[68] N. Jonić, I. Koprivica, C.M. Chatzigiannis, A.D. Tsiailanis, S.G. Kyrkou, E.P. Tzakos, A. Pavić, M. Dimitrijević, A. Jovanović, M.B. Jovanović, S. Marinho, I. Castro-Almeida, V. Otašević, P. Moura-Alves, A.G. Tzakos, I. Stojanović, Development of FluoAHRL: a novel synthetic fluorescent compound that activates AHR and potentiates anti-inflammatory T regulatory cells, Molecules 29 (13) (2024) 2988.
[69] M. Napolitano, C. Patruno, Aryl hydrocarbon receptor (AhR) a possible target for the treatment of skin disease, Med. Hypotheses 116 (2018) 96–100.
[70] E.H. van den Bogaard, G.H. Perdew, The enigma of AHR activation in the skin: interplay among ligands, metabolism, and bioavailability, J. Invest. Dermatol. 141 (6) (2021) 1385–1388.
[71] Z. Nie, C. Xiao, Y. Wang, R. Li, F. Zhao, Heat shock proteins (HSPs) in non-alcoholic fatty liver disease (NAFLD): from molecular mechanisms to therapeutic avenues, Biomark. Res. 12 (1) (2024) 120.
[72] C. Jonak, G. Klosner, F. Trautinger, Heat shock proteins in the skin, Int. J. Cosmet. Sci. 28 (4) (2006) 233–241.

Update

International Journal of Biological Macromolecules
Volume 319, Issue P1, August 2025, Page

DOI: https://doi.org/10.1016/j.ijbiomac.2025.145949

International Journal of Biological Macromolecules 319 (2025) 145949

Contents lists available at ScienceDirect

International Journal of Biological Macromolecules

journal homepage: www.elsevier.com/locate/ijbiomac

Corrigendum

Corrigendum to "Transformative lactera-polypyrrole@carrageenan microparticles leveraging NIR for skin regeneration and stress relief" [Int. J. Biol. Macromol. 2025 May 20: 144436]

Sih-Chi Chuang [a,b,1], Shih-An Yu [c,1], Pei-Chia Hung [c,1], Andrew E.-Y. Chuang [d,e,f,1], Jia-Wei Liang [c,d,1], Lekshmi Rethi [d,e,1], Chih-Kuang Chen [g,h,i], Hsu-Wei Fang [a], Hieu Trung Nguyen [j], Hsien-Tsung Lu [k,l,m,*]

[a] Department of Chemical Engineering and Biotechnology, National Taipei University of Technology, Taipei 10608, Taiwan
[b] Doctoral Program of Biochemical and Biomedical Engineering, National Taipei University of Technology, Taipei 10608, Taiwan
[c] Hsuan Chen Technology CO., LTD., New Taipei City 22055, Taiwan
[d] Graduate Institute of Biomedical Materials and Tissue Engineering, College of Biomedical Engineering, Taipei Medical University, New Taipei City, Taiwan
[e] International Ph.D. Program in Biomedical Engineering, College of Biomedical Engineering, Taipei Medical University, New Taipei City, Taiwan
[f] Cell Physiology and Molecular Image Research Center, Taipei Medical University-Wan Fang Hospital, Taipei 11696, Taiwan
[g] Department of Physical Medicine and Rehabilitation, Chang Gung Memorial Hospital, Taoyuan, Taiwan
[h] School of Medicine, Chang Gung University, Taoyuan, Taiwan
[i] Graduate Institute of Clinical Medicine, College of Medicine, Taipei Medical University, Taipei, Taiwan
[j] Department of Orthopedics and Trauma, Faculty of Medicine, University of Medicine and Pharmacy at Ho Chi Minh City, Ho Chi Minh City 700000, Viet Nam
[k] Department of Orthopedics, Taipei Medical University Hospital, Taipei City 11031, Taiwan
[l] Department of Orthopedics, School of Medicine, College of Medicine, Taipei Medical University, Taipei 11031, Taiwan
[m] International Ph.D. Program in Cell Therapy and Regenerative Medicine, College of Medicine, Taipei Medical University, Taipei 11031, Taiwan

"The authors regret that the normal group's merged image of Fig. 5b was misplaced. Please note that we have provided the correct Fig. 5b as below for better understanding. The authors stated that this correction do not change the validity of the work and scientific conclusions of this article."

Correct Figure

DOI of original article: https://doi.org/10.1016/j.ijbiomac.2025.144436.
* Corresponding author at: Department of Orthopedics, Taipei Medical University Hospital, Taipei City 11031, Taiwan.
E-mail address: lu7788@tmu.edu.tw (H.-T. Lu).
[1] These authors contributed equally.

https://doi.org/10.1016/j.ijbiomac.2025.145949

Available online 21 July 2025
0141-8130/© 2025 Elsevier B.V. All rights are reserved, including those for text and data mining, AI training, and similar technologies.

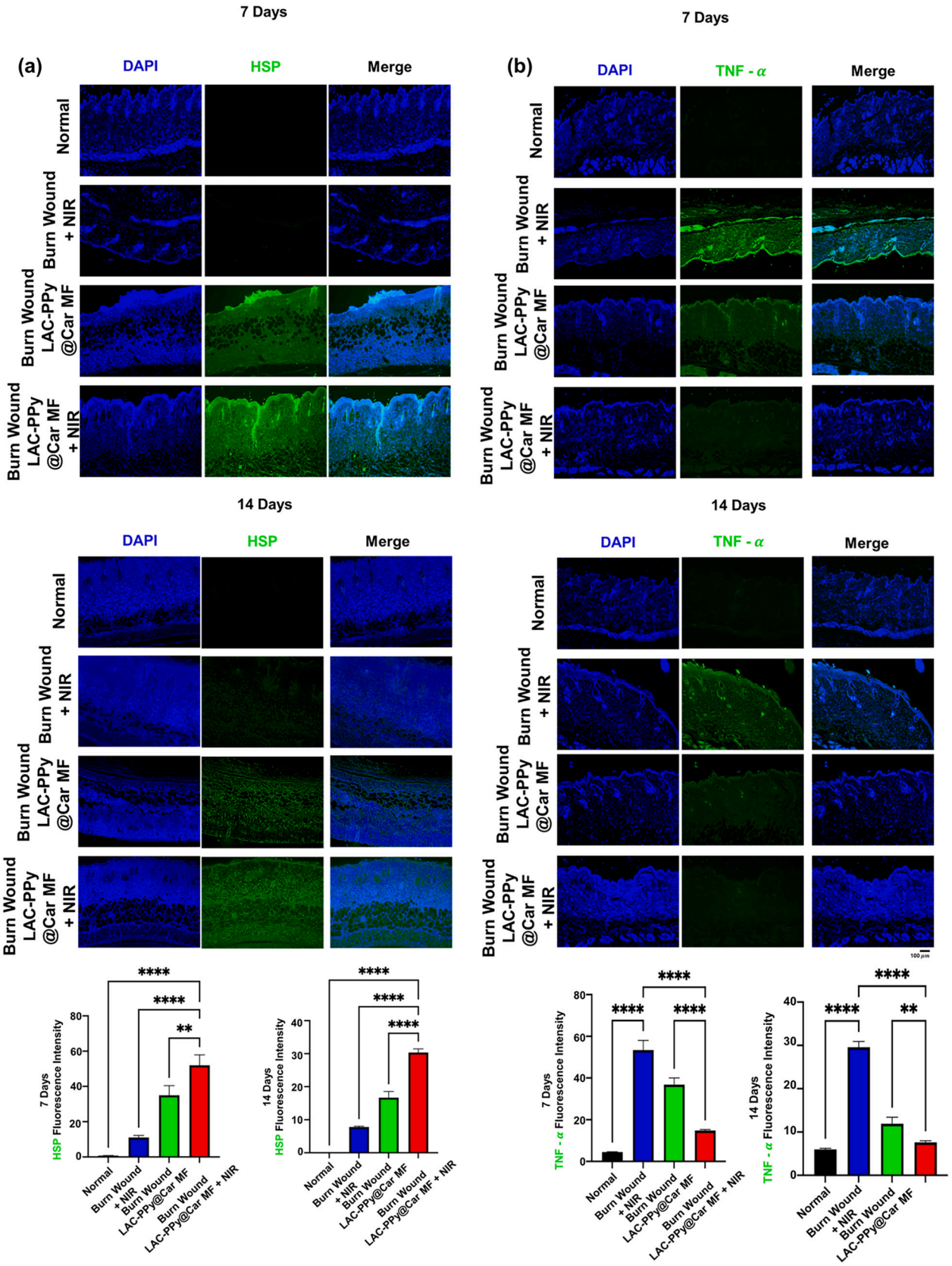

Fig. 5.

The authors would like to apologise for any inconvenience caused.